Hindawi
International Journal of Photoenergy
Volume 2021, Article ID 3981456, 12 pages
https://doi.org/10.1155/2021/3981456

Research Article

A Short-Term Solar Photovoltaic Power Optimized Prediction Interval Model Based on FOS-ELM Algorithm

G. Ramkumar,[1] **Satyajeet Sahoo**,[2] **T. M. Amirthalakshmi**,[3] **S. Ramesh**,[4] **R. Thandaiah Prabu**,[5] **Kasipandian Kasirajan**,[6] **Antony V. Samrot**,[7] **and A. Ranjith**[8]

[1]*Department of Electronics and Communication Engineering, Saveetha School of Engineering, SIMATS, Chennai, 602 105 Tamil Nadu, India*
[2]*Department of Electronics and Communication Engineering, Vignan's Foundation for Science, Technology and Research (Deemed to be University), Vadlamudi, Andra Pradesh, 522213, Guntur, India*
[3]*Department of Electronics and Communication Engineering, Rajalakshmi Institute of Technology, Chennai, Tamil Nadu, India*
[4]*Department of Electronics and Communication Engineering, St. Mother Theresa College of Engineering, Vagaikulam-628102, Tamilnadu, India*
[5]*Department of Electronics and Communication Engineering, Jeppiaar Institute of Technology, Chennai, Tamil Nadu, India*
[6]*Faculty of Engineering and Built Environment, Mahsa University, Malaysia*
[7]*School of Bioscience, Faculty of Medicine, Bioscience and Nursing, MAHSA University, Jenjarom, 42610 Selangor, Malaysia*
[8]*Department of Electronics and Communication Engineering, St. Joseph University in Tanzania, Dar es Salaam, Tanzania*

Correspondence should be addressed to G. Ramkumar; pgrvlsi@gmail.com and A. Ranjith; ranjith.arumugam@sjuit.ac.tz

Received 18 October 2021; Accepted 7 November 2021; Published 29 November 2021

Academic Editor: V. Mohanavel

Solar energy conversion efficiency has improved by the advancement technology of photovoltaic (PV) and the involvement of administrations worldwide. However, environmental conditions influence PV power output, resulting in randomness and intermittency. These characteristics may be harmful to the power scheme. As a conclusion, precise and timely power forecast information is essential for the power networks to engage solar energy. To lessen the negative impact of PV electricity usage, the offered short-term solar photovoltaic (PV) power estimate design is based on an online sequential extreme learning machine with a forgetting mechanism (FOS-ELM) under this study. This approach can replace existing knowledge with new information on a continuous basis. The variance of model uncertainty is computed in the first stage by using a learning algorithm to provide predictable PV power estimations. Stage two entails creating a one-of-a-kind PI based on cost function to enhance the ELM limitations and quantify noise uncertainty in respect of variance. As per findings, this approach does have the benefits of short training duration and better reliability. This technique can assist the energy dispatching unit list producing strategies while also providing temporal and spatial compensation and integrated power regulation, which are crucial for the stability and security of energy systems and also their continuous optimization.

1. Introduction

PV system research may bring solutions to the myriad difficulties confronting the location and the energy system itself. Trainings on improving the energy construction then enhancing the act of PV organization have been done [1]. Given the success mentioned previously, a PV system is especially sensitive to polluting and it has been disapproved for its instability, irregularity, and variable power generation. When the power supply was linked to the network, the situation of power fluctuations can threaten the network and endanger data security, making production scheduling much more challenging [2]. As a conclusion, reliable PV power production forecast is necessary in order to make improved generation suggestions, support temporal and spatial compensation, and provide synchronized control

scheme, lowering the requirement for power capacity and operational costs.

Many hybrid methods have been presented in recent years, combining the benefits of both methodologies. In reference, a hybrid technique depends on the wavelet transform (WT), and the radial basis function neural network (RBFNN) was created to anticipate short-term solar PV power. The annual autoregressive continuous simple moving approach was combined with the support vector machine (SVM) method by some researchers [3]. Given the fact that most of these methods, including the SVM and RBFNN designs, are significantly more challenging and informative for the network, they have been demonstrated to be real in the PV prediction.

The number of the approaches explored thus far ignored data time validation and presumed that the information does not seem out of date. In practice, training data must be updated in real time because it is time-dependent. So far, quite a few scientific papers have addressed this subject, among which was an online 24 hr forecasting method that employed RBF networks and classified input parameters depending on the type of weather [4]. Some of the academics have developed a two-stage process in which the solar power is statistically normalized first, and then, predictions of the standardized solar power were considered to anticipate PV power. Thus, we selected to use the extreme learning machine (ELM) method for the next reasons: ELM has a substantially lower computation complexion than many other machine learning techniques. ELM learns substantially quicker than most feed forward network learning techniques [5]. ELM outperforms many others in terms of generalization performance. The number of the hidden layer nodes is tiny and does not require tuning.

This study presents a novel strategy including the bootstrap technique, ELM, and improved DE (IDE) algorithm to generate optimum PIs for short-term PV power prediction [6]. The PIs addressed uncertainty in both predictive analysis and data disturbance at a quick rate, minimal computing burden, and good value for five-minute advanced PV power forecasts [7]. To begin, the bootstrap approach is being used to examine uncertainty in ELM models with the term of variance depending on ELM with PV power prediction. In addition, assumptions of data noises were the following: the frequency variation is evaluated but uses an ELM statistical model, the features of which have been optimized using an enhanced DE approach with a PI-based minimization problem.

Considering the variations of ELM equations, the information noise yields the optimum PIs with the coverage probability and the speed. Finally, the planned technique is shown through using an actual PV and atmospheric information from such a rooftop photovoltaic system [8]. The forecasting outcome shows that the suggested method is more dependable and effective than other ELM-based bootstrap methodologies. In order to anticipate PV power in various seasons, the ELM, OS-ELM, and FOS-ELM estimate models were tested. The results demonstrated that the FOS-ELM approach may expand accuracy while also reducing the training time.

2. Related Works

Ahn and Park provide a comprehensive RNN based on PV power estimate for the near future to identify the effect of climate deviations; the design employs an on-site climate IoT collection as well as actual power information. Thus, we investigated numerous limitations of the proposed deep RNN depending on prediction models; indeed, weather variables were grouped, in order to develop an effective predictive model. On the basis of the normalized RMSE, the accuracy rates of 5- and 15-minute forward solar PV power forecasts using three RNN networks with twelve time steps were 98.0 percent and 96.6 percent, consequently. Their individual R2 scores were 0.988 and 0.949. They performed 94.8 percent and 92.9 percent accuracy in studies 1 and 3 hours gaining the PV power predictions, correspondingly. Their R2 scores are 0.963 and 0.927, respectively. In these tests, the proposed deep RNN-based relatively brief prediction method outperformed the competition in terms of classification accuracy [9].

The purpose of this research is to employ intensity of light, air temperature, and humidity levels as input factors for determining solar output power. Considerations input data with wavelet soft beginning denoising to reduce noise and significantly increase the forecast model's adaptability in a variety of weather scenarios. Tented chaos patterning, asymmetric disturbances, and the multiple objective method were utilized to boost the whale algorithm's prediction performance; the revised whale algorithm was utilized to enhance the technique support vector machine (SVM) model for improving the forecast model's predictive performance. The study demonstrates that the symmetry-based long forecast model for solar panels achieves complete accuracy under a range of meteorological circumstances. The structured technique to predicting renewable output will promote the utilization of clean power and economic growth by reducing the burden of anticipating conversion efficiency [10].

One of the most critical concerns for the smart grid's effective and steady operation is solar photovoltaic fluctuations during the day. To adapt to PV power oscillations induced by climate changes, this work presents a short-term PV power forecasting method depending on the multilayer RNN. It is made up of multiple RNN layers that employ data from on-site IoT sensors to collect electricity and weather data. According to the normalized RMSE, the short-term PV power prediction accuracies of 5 minutes and 1 hour utilizing the 3 RNN layers with 12 time steps are 98.02 percent and 96.58 percent, respectively, according to empirical observations. The proposed short-term forecasting strategy based on the multi-RNN design was able to adjust the short-term PV power changes, as illustrated by these experimental results [11].

Solar power plants are a method of generating environmentally friendly renewable electricity, particularly in tropical areas where the sun shines all year. Rainfall, sun radiation, and clouds, on the other hand, can all have an effect on the maximum output of photovoltaic (PV) systems. Due to these considerations, establishing whether PV can

meet the current load's demands is challenging. This investigation advances a design to expect the output power of 160 × 285 W PV scheme in the topics when confident different situations are taken into account. To help forecast generation, the Python language is employed, together with one layer and multiple hidden layer multilayer perceptron, as well as typical multiple linear regression approaches. The simulation outcomes indicate that the neural network approach with two hidden layers surpasses one hidden layer and more linear regression in terms of reliability, as evaluated by R2, MSE, and MAE values [12].

Cervone et al. provide a method for creating 72-hour stochastic and deterministic estimates of the power produced by the photovoltaic (PV) power plants by utilizing input from the climate estimate, and quantifiable astronomical factors are based on Artificial Neural Networks (ANN) and Analog Ensemble (AnEn). ANN and AnEn are used to provide predictions for three photovoltaic panels in Italy, both separately and in combination. The computer flexibility of the planned method is assessed using synthetic data mimicking 4,450 PV power plants. The adequate manner of the suggested method is tested on the NCAR Yellowstone computer, which has nodes ranging from 1 to 4,450 [13].

3. Materials and Methods

3.1. Prediction Algorithm (Extreme Learning Machine (ELM)). The construction of ELM is displayed in Figure 1, and also, the procedure was explained below.

The ELM is an ANN with one hidden layer. The arbitrary hidden neuron quantity in the ELM design is assumed to be L, and distinct learning sample quantity (p, q) was supposed to be N [14]. Also, it is required which $p \in W^{d*N}, q \in W^{N}, x_k \in W^{1*d}, y_k \in W$, and x_k and y_k are both completely random arrays and vectors. The output function can then be rewritten:

$$f_H(p_n) = \sum_{k=1}^{H} \beta_k M(x_k, y_k, p_n) = q_n, \tag{1}$$

where β is the output weight matrix that links the randomized number of neurons to the output. G is the active purpose that joins the i^{th} arbitrary hidden neuron to the all-input nodes; then, this can be endlessly calculated as follows, such as the sigmoid function below:

$$M(x, y, p) = \frac{1}{1 + \exp\left(-(x \cdot p + y)\right)}. \tag{2}$$

Equation (1) can be expressed in the matrix form as

$$U \cdot \beta = P, \tag{3}$$

$$U = \begin{bmatrix} M(x_1, y_1, p_1) & \cdots & M(x_L, y_L, p_1) \\ \vdots & \ddots & \vdots \\ M(x_1, y_1, p_N) & \cdots & M(x_L, y_L, p_N) \end{bmatrix}, \tag{4}$$

$$\beta = [\beta_1 \ \beta_2 \quad \cdots \quad \beta_1]^T \ Q = [y_1 \quad y_2 \quad \cdots \quad y_N]^T.$$

The least-square approach to (1) is then

$$\beta = U^{+}Q = U^{T}\left(UU^{T}\right)Q, \tag{5}$$

which the matrix U represent the output hidden layer matrix, with i^{th} element (h_i) being the output hidden layer vector for the input p_i. Q is the vector containing training data's output. β is the only parameter that must be determined during the training procedure. The upper limit of the necessary number of distinct training models has several hidden nodes; the neurons in the hidden networks then will result in a lower subset of the training designs.

To applied regularization of parameter C to equation (5) to increase the stability and generalizability of the findings,

$$\beta = U^{T}\left(UU^{T} + \frac{1}{C}E\right)Q. \tag{6}$$

3.2. Online Sequential ELM (OS-ELM). The standard ELM implies that all information was being cast off for the training, whereas for estimate, information is sent chunk-by-chunk or one-by-one [15]. As a result, the traditional ELM must be modified to account for such circumstances. Historical climatic condition and PV power information were generated from the Supervisory Control and Data Acquisition (SCADA) structure on a regular basis and fed into the PV power forecast model. OS-ELM is better suited for PV power prediction because it refreshes the training data in real time. The algorithm is depicted below.

Step 1. Beginning—usage of a training data portion $\{(p_i, q_i)\}_{i=1}^{N_0}$ as initial information.

(i) Randomly produce p_j and q_j, where $j = 1, 2, \cdots, L$

(ii) Compute a primary hidden layer of the matrix output U_0:

$$U_0 = \begin{bmatrix} M(x_1, y_1, p_1) & \cdots & M(x_L, y_L, p_1) \\ \vdots & \ddots & \vdots \\ M\left(x_1, y_1, p_{N_0}\right) & \cdots & M\left(x_L, y_L, p_{N_0}\right) \end{bmatrix} \tag{7}$$

(iii) Approximation of the output initial weight vector:

$$\beta = U^{T}\left(UU^{T} + \frac{1}{C}E\right)Q, \tag{8}$$

Hindawi template version: may18

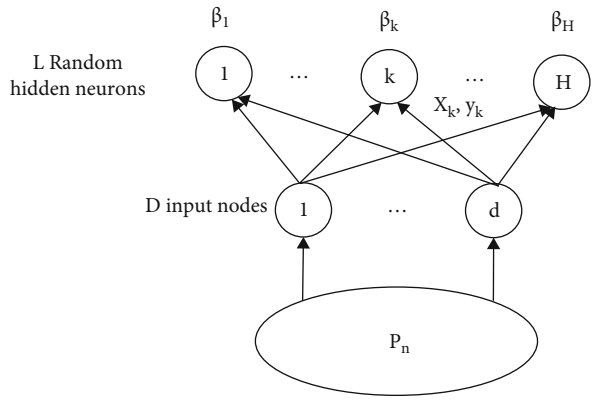

Figure 1: Extreme learning machine (ELM) architecture.

where

$$v_0 = \left(U_0^T U_0 + \frac{1}{C}E\right)^{-1},$$
$$Q_0 = \left[q_1 \cdots q_{N_0}\right]^T \tag{9}$$

(iv) Established $z = 0$

Online training.

(a) Once a $(z+1)^{\text{th}}$ new data portion $\{(p_i, q_i)\}_{i=(\sum_{j=0}^{z} N_j)+1}^{i=\sum_{j=0}^{z+1} N_j}$ is complete

(b) Compute the incomplete output hidden layer matrix U_{z+1} depending on the new data:

$$U_{z+1} = \begin{bmatrix} M\left(x_1, y_1, p_{\left(\sum_{j=0}^{z} N_j\right)+1}\right) & \cdots & M\left(x_L, y_L, p_{\left(\sum_{j=0}^{z} N_j\right)+1}\right) \\ \vdots & \ddots & \vdots \\ M\left(x_1, y_1, p_{z+1}_{\sum_{j=0} N_j}\right) & \cdots & M\left(x_L, y_L, p_{z+1}_{\sum_{j=0} N_j}\right) \end{bmatrix},$$
$$q_{z+1} = \begin{bmatrix} q_{\left(\sum_{j=0}^{z} N_j\right)+1} & \cdots & q_{z+1}_{\sum_{j=0} N_j} \end{bmatrix}^T \tag{10}$$

(c) Evaluation of the new q_{z+1} and $\beta^{(z+1)}$ based on

$$v_{z+1} = v_z - v_z U_{z+1}^T \left(I + U_{z+1} v_z U_{z+1}^T\right)^{-1} U_{z+1},$$
$$\beta^{(z+1)} = \beta^{(z)} + v_{z+1} U_{z+1}^T \left(p_{z+1} - U_{z+1}\beta^{(z)}\right) \tag{11}$$

Set $z = z + 1$, then start from Step 2.

3.3. OS-ELM with Forgetting Mechanism (FOS-ELM). The training information must be accessed within a specific time frame. In other words, information is only valid for a limited time [16]. Data received before a particular time in the FOS-ELM process can be not extendedly used lower than the forgetting mechanism; the obsolete information may make the prognosis less correct. Because of solar energy and temperatures varying seasonally, FOS-ELM is the better model for predicting PV power. The FOS-ELM technique is shown below.

Step 1. Configuration; this corresponds to the OS-ELM from Step 1.

Step 2. This process of forgetting is used in online learning.

When the $(z+1)^{\text{th}}$ new data chunk $\{(p_i, q_i)\}_{i=(\sum_{j=0}^{z} N_j)+1}^{i=\sum_{j=0}^{z+1} N_j}$ is prepared,

(a) compute the partially output hidden units' matrix U_{z+1}, for the most recent data

$$U_{z+1} = \begin{bmatrix} M\left(x_1, y_1, p_{\left(\sum_{j=0}^{z} N_j\right)+1}\right) & \cdots & M\left(x_L, y_L, p_{\left(\sum_{j=0}^{z} N_j\right)+1}\right) \\ \vdots & \ddots & \vdots \\ M\left(x_1, y_1, p_{z+1}_{\sum_{j=0} N_j}\right) & \cdots & M\left(x_L, y_L, p_{z+1}_{\sum_{j=0} N_j}\right) \end{bmatrix},$$

$$q_{z+1} = \left[q\left(\sum_{j=0}^{z} N_j\right)+1 \quad \cdots \quad \sum_{j=0}^{q_{z+1}} N_j \right]^T \tag{12}$$

(b) calculate the new q_{z+1} and β^{th} based on

$$v_{z+1} = v_z - v_z \begin{bmatrix} -U_{z-e-1} \\ U_{z+1} \end{bmatrix}^T \times \left(I + \begin{bmatrix} U_{z-e-1} \\ U_{z+1} \end{bmatrix} v_z \begin{bmatrix} -U_{z-e-1} \\ U_{z+1} \end{bmatrix}^{T^{-1}} \right) \times \begin{bmatrix} U_{z-e-1} \\ U_{z+1} \end{bmatrix} v_z,$$

$$\beta^{(z+1)} = \beta^{(z)} + v_{z+1} \begin{bmatrix} -U_{z-e-1} \\ U_{z+1} \end{bmatrix}^T \times \left(\begin{bmatrix} q_{z-e-1} \\ q_{z+1} \end{bmatrix} - \begin{bmatrix} U_{z-e-1} \\ U_{z+1} \end{bmatrix} \beta^{(z)} \right) \tag{13}$$

(c) set as $z = z + 1$, then go back to Step 2

The integration of the forgetting mechanism, which could not get rid of the obsolete prevent information of their involvement in opportunities online and also show the timeliness of the data, is the evident difference between FOS-ELM and OS-ELM.

3.4. PI Structure and Valuation

3.4.1. Formulation of PI. Assuming a training sample selected $S = \{(p_i, t_i)_{i=1}^N\}, p_i p_i$ is an input dataset containing historical data [6]. It is 5-minute gaining of PV power, which is used as the benchmark. PIs were built that contain the goal t_i with given assurance level $(1-\alpha)$, known as PI nominal confidence (PINC) $100(1-\alpha)\%$, percent, and PIs $M_t^\alpha(p_i)$ can be defined for the i^{th} target as

$$M(p_i) = [L(p_i), U(p_i)], \tag{14}$$

where $L(p_i)$ and $U(p_i)$ signify PI lower bounds and upper bounds, respectively. The PI attention amount can be defined as

$$x(t_i \in [L(p_i), U(p_i)]) = 100(1-\alpha)\%. \tag{15}$$

t_i is the i^{th} target measured; this can be well defined as

$$t_i = q(p_i) + \mu(p_i) = f(p_i, \vartheta) + \varepsilon(p_i), \tag{16}$$

where $q(p_i)$ is the genuine regression average and $\varepsilon(p_i)$ is the mean noise with a zero mean. $f(p_i, \vartheta)$ is a mapping among the input p_i and exact regress value $q(p_i)$. The ELM technique is used as a regression design in this paper to approximate the true return value. As a result, the mean of the accurate regression $q(p_i)$ can be approximated by the output of the ELM model $f(p_i, \widehat{\vartheta})$:

$$\widehat{q}(p_i) = f(p_i, \vartheta) = E\left(\frac{t_i}{p_i}\right), \tag{17}$$

where $\widehat{q}(p_i)$ denotes a prediction target value; the prediction error can be defined as

$$t_i - \widehat{q}(p_i) = [q(p_i) - \widehat{q}(p_i)] + \varepsilon(p_i), \tag{18}$$

where $t_i - \widehat{q}(p_i)$ represents the overall error of prediction and reflects difference among the measured value t_i and value of real estimate $\widehat{q}(p_i)$. The error between the expected true regression output as well as the observed ELM output is denoted by $[q(p_i) - \widehat{q}(p_i)]$ denoting noise with such a mean of zero [17]. PIs are built to measure uncertainties in overall prediction, which consists of two independent statistical parts: $[q(p_i) - \widehat{q}(p_i)]$ and $\varepsilon(p_i)$. As a result, the total variance is defined as

$$\sigma_t^2(p_i) = \sigma_{\widehat{q}}^2(p_i) + \sigma_\varepsilon^2(p_i), \tag{19}$$

where $\sigma_{\widehat{q}}^2(p_i)$ is the model uncertainty variance and $\sigma_\varepsilon^2(p_i)$ is the information uncertainty variance. The low bound $L_t^\alpha(p_i)$ and upper bound $U_t^\alpha(p_i)$ can be rewritten as

$$L_t^\alpha(p_i) = \widehat{q}(p_i) - r_{1-\alpha/2}\sqrt{\sigma_{\widehat{t}}^2(p_i)}, \tag{20}$$

$$U_t^\alpha(p_i) = \widehat{q}(p_i) + r_{1-\alpha/2}\sqrt{\sigma_{\widehat{t}}^2(p_i)}, \tag{21}$$

where $r_{1-\alpha/2}$ is the $1-\alpha/2$ standard normal quantile distribution.

3.4.2. PI Quality Metrics. The likelihood of PI coverage (PICP) and the breadth of PIs are two important indicators. The number of metrics and the indicators are presented to assess the quality of PIs [18]. The most essential metric for measuring the dependability of the PIs is PICP, which value reflects the likelihood that PIs will cover the upcoming objective. A greater value of PICP specifies that perhaps PIs are much more likely to accomplish the required area. For N labeled data, PICP is calculated as

$$\text{PICP} = \frac{1}{N}\sum_{t}^{N} \delta_t, \tag{22}$$

where δ_t is the Boolean value that can be given as

$$\delta_t = \begin{cases} 1, & t_i \in M_i^\alpha, \\ 0, & t_i \in M_i^\alpha. \end{cases} \tag{23}$$

Another essential metric for assessing the quality of the PIs is the interval breadth. If ignoring the interval width and only considering the PICP, and even if a high PICP

value is attained, it is difficult for decision-makers to gain relevant forecasting data. As a conclusion, better quality PIs must take PICP and PI quality into account totally. The brightness of PIs could be calculated using the mean prediction interval width (MPIW):

$$\text{MPIW} = \frac{1}{NE}\sum_{i=1}^{N}(U_t^{\alpha}(p_i) - L_t^{\alpha}(p_i)), \tag{24}$$

where E is a target variety and N is the number of datasets.

3.4.3. Model Uncertainty Variance. In 1979, the bootstrap technique is presented and named as a resampling methodology. Because of its simplicity and resilience, it is commonly used to predict a fundamentally unknown probability using a likelihood function. Bootstrap methods are used in regression applications to assess the uncertainty of regression models [19]. It is utilized in this study to quantify the uncertainty in the ELM model induced by the construction misspecification and arbitrarily assigned to the parameters of input. The variance is used to illustrate the uncertainty in the model.

An original training information model can be well defined as $D_{\text{orin}} = \{(p_i, t_i)\}_{i=1}^{N*}$ for the paired bootstrap approach, and the B training subdatasets $D_{\text{sub}} = \{(p_i, t_i)\}_{i=1}^{N*}$ are uniformly resampled using D_{orin} by replacing. Each ELM model's output is $\widehat{q}_s(p_i)$. The mean of the bootstrap ELM outputs can be used to estimate the genuine regression value. It can be represented as follows for B ELM models:

$$\widehat{q}(p_i) = \frac{1}{B}\sum_{s=1}^{B}\widehat{q}_s(p_i). \tag{25}$$

Depending on the B period ELM assessed findings, modification of design uncertainty is stated as

$$\sigma_{\widehat{q}}^2(p_i) = \frac{1}{B-1}\sum_{s=1}^{B}(\widehat{q}_s(p_i) - \widehat{q}(p_i)). \tag{26}$$

3.5. Architecture Model

3.5.1. Model. An array's PV output energy is measured as

$$p_s = \eta DR[1 - e(t_0 - 25)], \tag{27}$$

while η is the convert productivity, D is the array dimension PV (m^2), R is the solar energy (kW/m^2), e is the array effectiveness damage for every degree Celsius increase in the cell temperature, and t_0 is the ambient temperature (°C).

From equation (27), several parameters influence output power, including PV array dimensions, transform efficiency, ambient temperature, and solar radiation.

3.5.2. Input Vector. Based on its physical model offered, the elements that control output power are determined. As illustrated in the historical statistics, the effectiveness and dimensions of a multidimensional sequence are fixed. Ultraviolet irradiance and climatic parameters, on the other hand, change on a routine basis. As a consequence, as input parameters, choose time, radiation from the sun, and ambient temperature. A numerical weather prediction (NWP) technique is utilized to gather the input data [20]. It forecasts the temperature using computational equations of the composition of the atmosphere based on the changing meteorological conditions. The following is the source image:

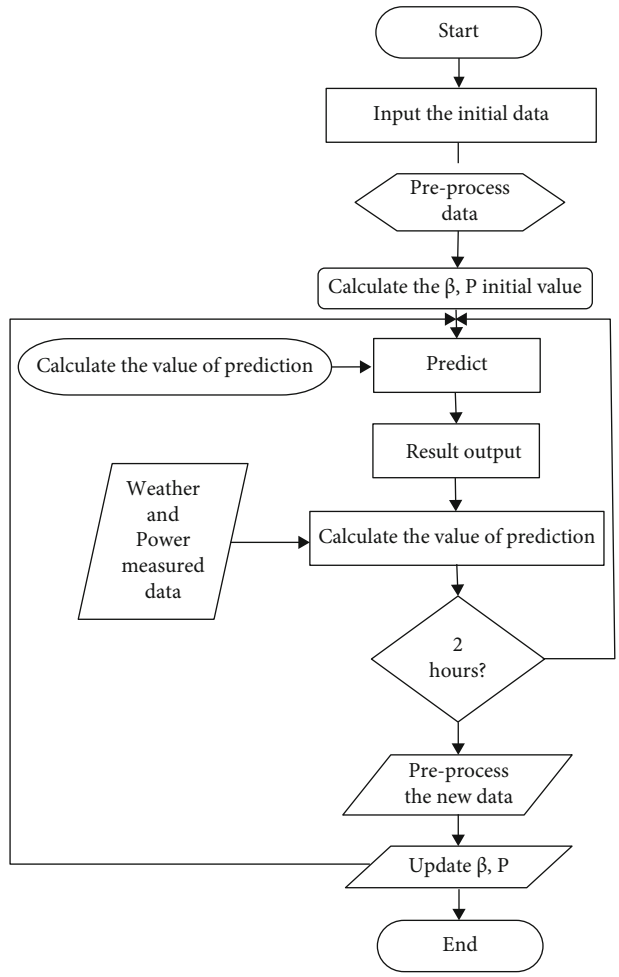

Figure 2: Flowchart prediction system for online sequential extreme learning machine with forgetting mechanism (FOS-ELM).

$$p_i = [\text{time temp } R]^T. \tag{28}$$

If temperature is the environmental temperatures, R seems to be the solar irradiance attainment region of the planet's surface closest to the PV cells.

3.6. Preprocessing Data. When standardizing various variables that adjust to the ELM in the following:

$$\overline{p_i} = \frac{p_i - p_{\min}}{p_{\max} - p_{\min}}, \tag{29}$$

where p_i denotes the input or output information and $p_{\max}$ and $p_{\min}$ denote the highest and smallest values. Since results

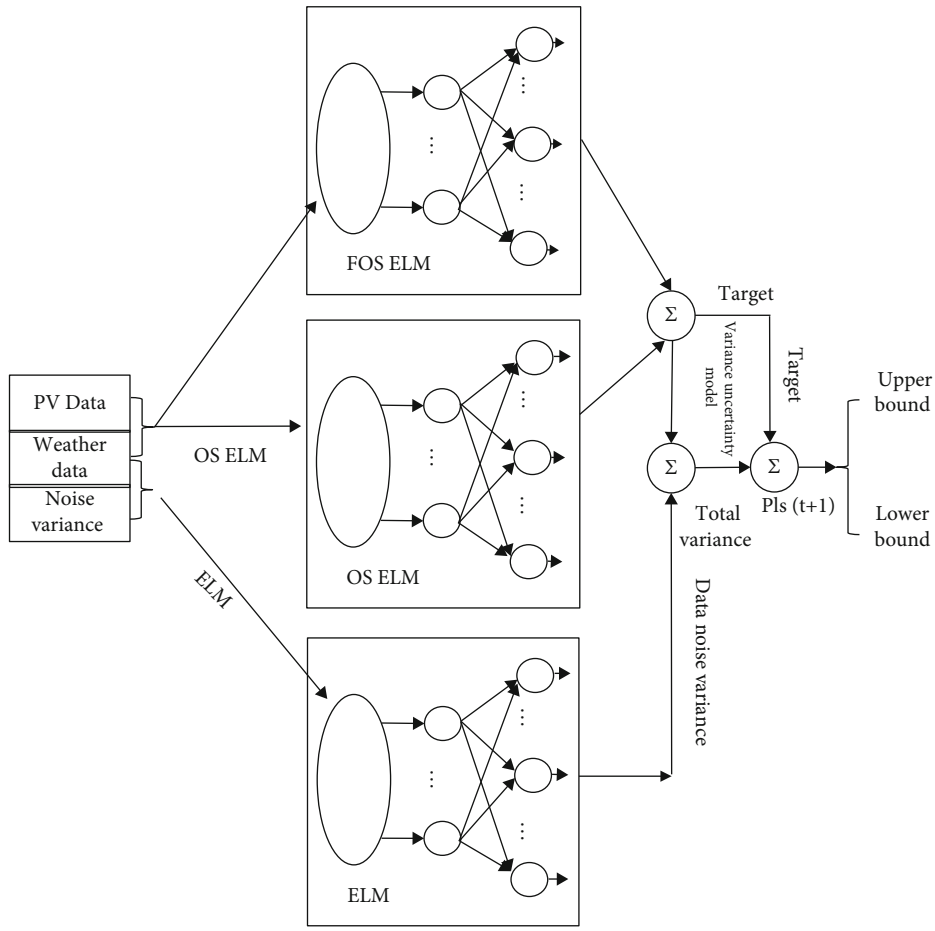

Figure 3: Proposed diagram.

obtained could be perfect, estimated power generation and direct solar information may possibly be below zero outstanding to statistical faults, which really was unachievable in the practice. In this case, change both to zero and also the corresponding expected data. After computing the faults, the data set shall be destroyed if the predicted and measured numbers are also both equivalent to 0.

3.7. Error Evaluation. The prediction algorithms were evaluated using the normalized Root Mean Square Error (nRMSE) and a Mean Absolute Percent Error (MAPE) [21]; these are evaluated as follows:

$$\text{nRMSE} = \frac{1}{V_{\text{rated}}} \sqrt{\frac{1}{n} \sum_{i=1}^{n} (V_{ui} - V_{vi})^2}, \tag{30}$$

$$\text{MAPE} = 100 \times \frac{1}{n} \sum_{i=1}^{n} \frac{|V_{mi} - V_{vi}|}{V_{mi}}, \tag{31}$$

where n represents the total number of power generation on the time periods, P_{rated} represents rated power, V_{vi} represents anticipated energy in the i^{th} time period, and V_{mi} represents the calculated influence in the i^{th} period. Researchers excluded the information established since together solar energy and PV power generated were equivalent to 0 by excluding night information.

3.8. Model Flowchart. The development of estimate is demonstrated in Figure 2. First, enter the early available information for preprocessing, then create the primary output hidden layer matrix H_0 and predict β_0 and P_0. Then, input forecasts over the next few days and calculate the predictive model [5]. When statistical information such as climate and electricity data come, they evaluate the forecast inaccuracy and save the data. Then take a glance at the moment. If it equals 1 h, inform the conditions H, β, and P; then, a preceding procedure was constant.

3.9. PI-Based Cost Function. The variance of noise is evaluated using the standard bootstrap approach under the presumption that information noise is dispersed generally with a zero mean. To train ELM parameters, the cost function of the maximum likelihood approximation is employed rather than one developed by employing assessment indicators of the complete PI presentation [22]. As a result, standard PIs are not always able to find the best PIs. To address this problem, this work proposes a new PI-based cost function that receives the PICP and the break length into a consideration to calculate data error variance.

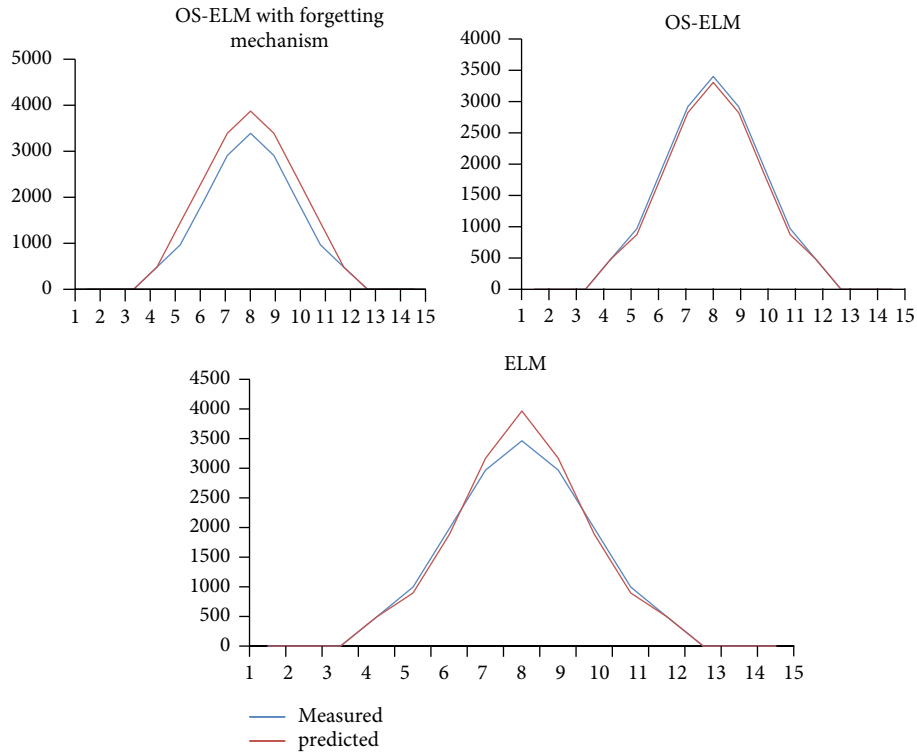

Figure 4: Sunny day three-model comparison.

PI performance should be evaluated in two ways: MPIW and PICP. It is pointless if only one component of PI performance is presented. A coverage width-based criterion (CWC) is specified as a PI-based cost function:

$$\mathrm{CWC} = \mathrm{MPIW} + \gamma \mathrm{PICP}^{\lambda} \times |\mu - \mathrm{PICP}|, \tag{32}$$

where m is the specified probability which is equivalent to the PI nominal confidence (PINC) level of $100(1-\alpha)\%$. l is a hyperparameter with a value among 10 and 100 that is used to penalize invalid PIs and γPICP. In this paper, the CWC value is normalized by nominal PV power and given as a percentage. A higher performing PI has been accomplished if a lower value of CWC is produced at the specified confidence level on $100(1-\alpha)\%$, which is the purpose of the PICP. If the rate of PICP is much added than m, γPICP worth is set to be 0, then the CWC rate is decided by the MPIW, which indicates that the breadth of the PIs must be preserved. Then, the PICP value was much fewer than m, the γPICP value is set to be 1, then the CWC is a total of the together MPIW then $\lambda * |\mu - \mathrm{PICP}|$, representing that broader PIs would be found to obtain an additional acceptable value of the PICP. In this paper, the CWC value was regularized by the minimal PV power and given as a percentage. A higher performing PI has been accomplished if a lower value of CWC is produced at the assumed assurance level on $100(1-\alpha)\%$.

Figure 3 depicts how the recommended fluctuation of unknown parameters and data disturbances is averaged to create PIs. This is vital to create an exact estimation modification of information disturbance in order to construct appropriate PIs. In this paper, an ELM model is constructed to predict the unpredictability of information disruption, so this improved DE (IDE) is used to enhance the ELM number of the criteria by diminishing a CWC [23]. As a result, as described by equation (32), the PI-based objective function for IDE is presented as follows:

$$F = \text{minimum}\,(\mathrm{CWC}). \tag{33}$$

The limitations can be well defined as

$$U(p) > L(p) \geq 0, \tag{34}$$

$$\begin{cases} \text{if } \alpha_i \leq \alpha_j, \\ L^{\alpha_i}(p) \geq L^{\alpha_j}(p),\ U^{\alpha_i}(p) \geq U^{\alpha_j}(p). \end{cases} \tag{35}$$

The first of the two restrictions are automatically fined with that as long as the computation is correct [24]. The other implies that given the identical datasets, a lower confidence level $(1\,a)$ should result in wider PIs.

3.10. Procedures. The proposed method can be separated into two sections in general. The following is a description of the detailed procedure. The bootstrap technique is used in the first stage to determine the modification of model uncertainty.

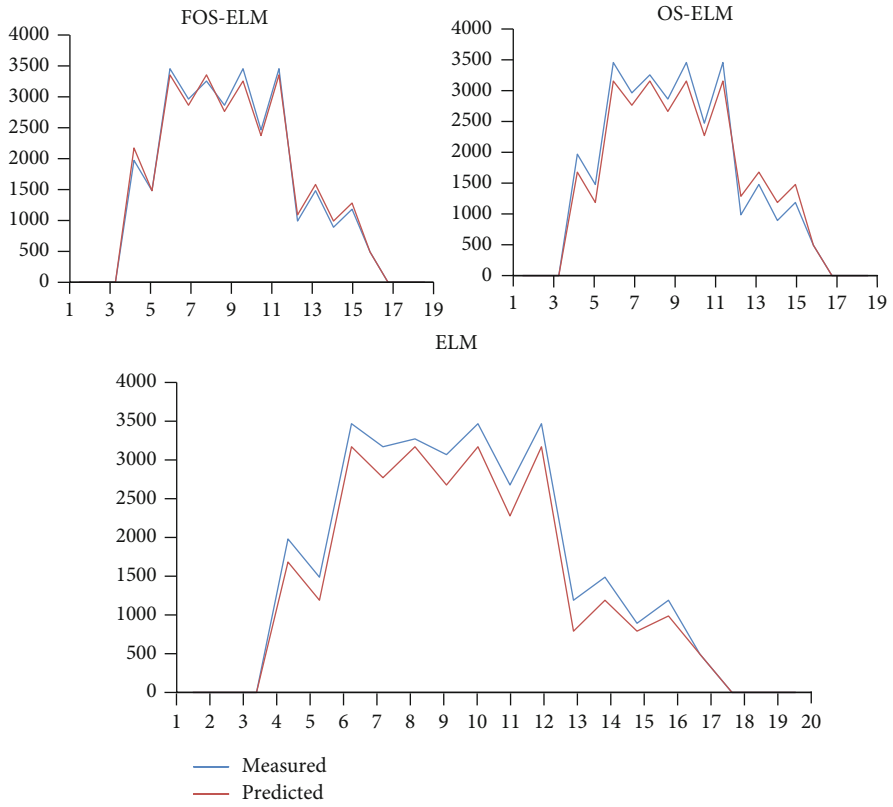

Figure 5: Cloudy/rainy day: three-model comparison.

Step 1. Resample $D_{\text{sub}} = \{(p_i, t_i)\}_{i=1}^{N*}$ B training models by the replacement from innovative PV training dataset $D_t = \{(p_i, t_i)\}_{i=1}^{N}$.

Step 2. Using the model of ELM regress, predict each trained model and produce $\{\widehat{q}_s(p_i)\}_{s=1}^{B}$.

Step 3. Equations (24) and (25) are used to calculate the mean output of the B ELMs models $\widehat{q}_s(p_i)$ and the alteration of the model uncertainty $\sigma_q^2(p_i)$ based on Step 2.

Step 4. $D_{r^2} = \{p_i, r^2(p_i)\}_{i=1}^{N}$ is the residual sample.

The 2nd stage's goal is to evaluate a modification of the information noise and build appropriate PIs.

To estimate variance of the data noise, an ELM approach was used [25]. Because ELM's input weight and hidden layers are generated at random, it is inescapable that most of them are the nonoptimal values. Furthermore, it has been demonstrated that the presentation of ELM is dependent on the excellence of the input masses and the concealed biases. The algorithm of IDE was utilized to identify the best ELM parameters by minimalizing the PI-based cost function in order to acquire the optimum PIs.

Step 1. The population is generated at random, and the applicant solution s_i is made up of a collection of input weights and hidden biases; i^{th} each can be expressed as

$$s_i = [C_{11}, \cdots, C_{1L}, C_{21}, \cdots, C_{2L}, \cdots, C_{n1,} C_{nL}, y_1, \cdots, y_n]. \quad (36)$$

Table 1: Evaluation of the monthly average accuracy comparison.

Climatic condition	Technique	nRMSE	MAPE
Winter season	ELM	0.984	1.770
	FOS-ELM	0.876	1.524
	OS-ELM	0.943	1.631
Autumn season	ELM	0.975	1.793
	FOS-ELM	0.893	1.528
	OS-ELM	0.934	1.632
Summer season	ELM	1.084	1.603
	FOS-ELM	0.893	1.432
	OS-ELM	0.934	1.584
Spring season	ELM	1.127	1.848
	FOS-ELM	0.952	1.549
	OS-ELM	1.042	1.673

Table 2: Comparison of test period and training period.

Technique	Training period (sec)	Test period (sec)
FOS-ELM	0.052	0.095
OS-ELM	0.052	0.049
ELM	0.076	0.076

Table 3: Comparison of different PIs on various climatic conditions.

Climatic condition	PINC(%)	Determination	Bootstrap-based traditional NNs (BNNs)	Double bootstrap method	Bootstrap MLE method	Bootstrap ELM method
Northeast monsoon	90%	19.06	15.19	14.32	14.25	13.76
Intermonsoon	90%	14.89	12.57	12.45	12.30	12.09
Southwest monsoon	90%	20.08	13.65	12.15	12.04	12.02
Intermonsoon	90%	26.55	15.89	13.14	13.03	12.65

Step 2. Each particular population is made up of a set of weights and hidden biases. Equation (2) is used to calculate the corresponding output weights, and $\delta_{\varepsilon}^{2}(p_i)$ is estimated.

Step 3. Use equation (19) to compute the total variance $\delta_{t}^{2}(p_i)$ and equations (20) and (21) to calculate the lower bound $\widehat{L}_{t}^{\alpha}(p_i)$ and upper bound $\widehat{U}_{t}^{\alpha}(p_i)$.

Step 4. The suitability of cost function, CWC, may be determined using equations (32), (22), and (24).

Step 5. An enhanced ID method is designed to alter ELM parameters in order to acquire the best s $\delta_{\varepsilon}^{2}(p_i)$ depending on the neutral function equation (33) and restriction equations (32) and (34).

Step 6. Steps 5 and 3 are used to construct the PIs.

4. Result and Analysis

Research emphasizes on the evaluation of the FOS-ELM, ELM, and OS-ELM because an ELM technique has a shorter development time and increased accuracy rate than BP neural nets, as shown in the research. The following are the specifics for the three models:

Model 1:(algorithm of FOS-ELM). the sigmoidal activation function is chosen as the method that can solve; results collected 48 hours prior to the current time were utilized as test examples to anticipate its energy production; the training model was adjusted every hour, but the information collected 48 hours prior got eliminated.

Model 2:(algorithm of OS-ELM). the exponent is being used as the dynamic variable; data received 48 hours prior to kick-off was used as the train approach to estimate electrical output; quality management was updated every hour utilizing the historic information that was still accessible.

Model 3:(ELM algorithm). the sigmoidal activation purpose is selected as greatly exceeding, and evidence gathered over the preceding month's past 48 hours was used to estimate power output. To put it another way, the algorithms were trained monthly.

Table 4: Comparison of test period and training period.

Technique	Training period (sec)	Test period (sec)
BNN bootstrap	0.0857	0.0574
MLE bootstrap	0.0138	0.0424
Double bootstrap	0.0147	0.0837
ELM bootstrap	0.0135	0.0422

4.1. Single-Day Accuracy Comparison. A three-model comparison predicted outcomes in a particularly sunny day in Figure 4. Figure 5 shows the three model comparison predicted outcomes in a Cloudy/rainy day.

Models 3, 2, and 1 have nRMSEs of 0.024, 0.036, and 0.054, respectively, and MAPEs of 9.708, 10.893, and 12.706. The precision of Prototypical 1 is clearly the best of the 3 models. Models 1, 2, and 3 have nRMSEs of 0.068, 0.075, and 0.083, correspondingly; the related MAPEs are 13.834, 14.304, and 15.112. Model 1's precision remains unquestionably the greatest of the three variants. Furthermore, by associating Figures 3 and 4, we can observe that the precision is higher when it becomes hotter than if it is foggy or wet.

4.2. Average Accuracy of Monthly Comparison. To assess the precision of three systems in various periods, data from the spring, summer, autumn, and winter seasons were used for the study. Table 1 summarizes the findings.

Table 1 demonstrates that the prediction correctness is better in the summers and the winters than in the autumn season in terms of nRMSE; the model has the best precision, while Model 3 has the lowest precision. In terms of MAPE, summer accuracy is better than winter accuracy; once again, Model 1 takes the precision value and Model 3 has the deepest. In conclusion, the strategy of FOS-ELM surpasses all others.

4.3. Training Time Comparison. In Model 1, startup takes 0.095 seconds and online training takes 0.052 seconds. Model 2 takes the same amount of time to initialize as Model 1, but only 0.049 seconds for online study. In Model 3, training takes 0.076 seconds each time as shown in Figure 5. As a result, it can be demonstrated that an online course saves approximately 30% of the retrain period. But, every time an online study is undertaken, Model 1 takes 6% longer than Model 3. Table 2 summarizes the comparison of test and training period.

The level of uncertainty in PV generation is strongly related to the chaotic nature of weather schemes. The

weather and solar radiation patterns change dramatically throughout the year. The warmer temperatures are considered by the two southwest monsoons divided by the intermonsoonal periods. Four seasons in Singapore are explored to validate the performance of the suggested approach: The northeast monsoon season (December to March), the intermonsoon period (April to May), the southwest monsoon season (June to September), and the intermonsoon period (October–November) were the four periods. The equivalent model is created for individual seasons. The equivalent model was created for each season. When the periodic differences and diversity are taken into account, the northeast monsoon, the intermediate monsoon, the southeastern monsoon, and the intermonsoon are chosen to generate test datasets to validate the proposed approach, and the remaining data are used as training datasets. Table 3 summarizes the findings with different PIs.

From Figure 2, the determination technique, the double bootstrap method, and MLK bootstrap technique are all outperformed by the approach. The nominal certainty increases as the PICP value rises. It means that the PIs have a better chance than the average profit of replacing the PV power in the next 5 minutes. When contrasted to the extra deadlifting models, the technique had the extreme value of PICP. Furthermore, the proposed approach's MPIW values are lower than those of previous benchmarking models. It demonstrates that the strategy resulted in smaller intervals. Comparison results shown in Table 4.

5. Conclusion

A new interim model of PV power forecast on the FOS-ELM approach is used in this work. To begin, they gave a fast summary of ELM, OS-ELM, and FOS-ELM theories, as well as the distinctions between the various theories to describe; FOS-ELM was the ideal approach that estimates generation of PV power. Now, this approach could be used for the practical purpose as a prediction device. Short-term forecasting of solar output is critical for power system functioning and economic cost. For quantifying the uncertainties in the PV power group, an extreme learning machine (ELM) and the model of bootstrap have been used along with the approach on the short-term PI forecasting method. Mutually, the data noise and the model of regression have been used to build the PI model. The bootstrap method is used to detect uncertainty of ELM systems, and a hybrid approach of the ELM and IDE with a PI optimal pricing purpose is built to estimate assumptions of the data noise. The suggested methodology could be more than 60 times nearer in training and 10 times nearer in evaluating than the BNNs, showing that the recent theories have great online possibility for the short-term power producing forecasts.

Data Availability

The data used to support the findings of this study are included within the article.

Conflicts of Interest

The authors declare that there is no conflict of interest regarding the publication of this article.

Acknowledgments

The authors would like to express their gratitude towards Saveetha School of Engineering, Saveetha Institute of Medical and Technical Sciences (formerly known as Saveetha University), for providing the necessary infrastructure to carry out this work successfully.

References

[1] M. Rana, I. Koprinska, and V. G. Agelidis, "Univariate and multivariate methods for very short-term solar photovoltaic power forecasting," *Energy Conversion and Management*, vol. 121, pp. 380–390, 2016.

[2] G. Ramkumar, S. Sahoo, G. Anitha et al., "An unconventional approach for analyzing the mechanical properties of natural fiber composite using convolutional neural network," *Advances in Materials Science and Engineering*, vol. 2021, Article ID 5450935, 15 pages, 2021.

[3] S. Mahesh and G. Ramkumar, "Smart face detection and recognition in low resolution images using Alexnet CNN compare accuracy with SVM," *Alinteri Journal of Agriculture Sciences*, vol. 36, no. 1, pp. 721–726, 2021.

[4] G. Ramkumar, M. Ayyadurai, and C. Senthilkumar, "An effectual underwater image enhancement using deep learning algorithm," in *2021 5th International Conference on Intelligent Computing and Control Systems (ICICCS)*, pp. 1507–1511, 2021.

[5] G. Ramkumar and E. Logashanmugam, "Study on impulsive assessment of chronic pain correlated expressions in facial images," *Biomedical Research*, vol. 29, no. 16, 2018.

[6] Q. Ni, S. Zhuang, H. Sheng, S. Wang, and J. Xiao, "An optimized prediction intervals approach for short term PV power forecasting," *Energies*, vol. 10, no. 10, p. 1669, 2017.

[7] Z.-H. Li, J.-J. Yang, H.-Q. Qin, Y.-W. Xia, and M. Zhuang, "A study of efficiency evaluation of national quality online courses during the epidemic: based on fuzzy logic calculation and bootstrap-DEA," *Mathematical Problems in Engineering*, vol. 2021, Article ID 5534583, 7 pages, 2021.

[8] H. Zhang, S. Zhang, and Y. Yin, "Online sequential ELM algorithm with forgetting factor for real applications," *Neurocomputing*, vol. 261, pp. 144–152, 2017.

[9] H. K. Ahn and N. Park, "Deep RNN-based photovoltaic power short-term forecast using power IoT sensors," *Energies*, vol. 14, no. 2, p. 436, 2021.

[10] Y.-W. Liu, H. Feng, H.-Y. Li, and L.-L. Li, "An improved whale algorithm for support vector machine prediction of photovoltaic power generation," *Symmetry*, vol. 13, no. 2, p. 212, 2021.

[11] N. Park and H. K. Ahn, "Multi-layer RNN-based short-term photovoltaic power forecasting using IoT dataset," in *2019 AEIT International Annual Conference (AEIT)*, pp. 1–5, Florence, Italy, 2019.

[12] R. Azka, W. Soefian, D. R. Aryani, F. H. Jufri, and A. R. Utomo, "Modelling of photovoltaic system power prediction based on environmental conditions using neural network single and

multiple hidden layers," in *IOP Conference Series: Earth and Environmental Science*, vol. 599, 2020.

[13] G. Cervone, L. Clemente-Harding, S. Alessandrini, and L. Delle Monache, "Short-term photovoltaic power forecasting using artificial neural networks and an analog ensemble," *Renewable Energy*, vol. 108, pp. 274–286, 2017.

[14] Y. Dash, S. K. Mishra, and B. K. Panigrahi, "Rainfall prediction for the Kerala state of India using artificial intelligence approaches," *Computers & Electrical Engineering*, vol. 70, pp. 66–73, 2018.

[15] W. Mao, J. Wang, and Z. Xue, "An ELM-based model with sparse-weighting strategy for sequential data imbalance problem," *International Journal of Machine Learning and Cybernetics*, vol. 8, no. 4, pp. 1333–1345, 2017.

[16] D. Xiao, B. Li, and S. Zhang, "An online sequential multiple hidden layers extreme learning machine method with forgetting mechanism," *Chemometrics and Intelligent Laboratory Systems*, vol. 176, pp. 126–133, 2018.

[17] W. Kong, Z. Y. Dong, Y. Jia, D. J. Hill, Y. Xu, and Y. Zhang, "Short-term residential load forecasting based on LSTM recurrent neural network," *IEEE Transactions on Smart Grid*, vol. 10, no. 1, pp. 841–851, 2017.

[18] I. Serykh and D. Sonechkin, "Nonchaotic and globally synchronized short-term climatic variations and their origin," *Theoretical and Applied Climatology*, vol. 137, no. 3, pp. 2639–2656, 2019.

[19] C. Wan, Z. Xu, P. Pinson, Z. Y. Dong, and K. P. Wong, "Probabilistic forecasting of wind power generation using extreme learning machine," *IEEE Transactions on Power Systems*, vol. 29, no. 3, pp. 1033–1044, 2013.

[20] J. Wang, P. Li, R. Ran, Y. Che, and Y. Zhou, "A short-term photovoltaic power prediction model based on the gradient boost decision tree," *Applied Sciences*, vol. 8, no. 5, p. 689, 2018.

[21] Z. Li, L. Ye, Y. Zhao, X. Song, J. Teng, and J. Jin, "Short-term wind power prediction based on extreme learning machine with error correction," *Protection and Control of Modern Power Systems*, vol. 1, no. 1, pp. 1–8, 2016.

[22] A. Khosravi, S. Nahavandi, D. Srinivasan, and R. Khosravi, "Constructing optimal prediction intervals by using neural networks and bootstrap method," *IEEE transactions on neural networks and learning systems*, vol. 26, no. 8, pp. 1810–1815, 2014.

[23] Q. Ni, S. Zhuang, H. Sheng, G. Kang, and J. Xiao, "An ensemble prediction intervals approach for short-term PV power forecasting," *Solar Energy*, vol. 155, pp. 1072–1083, 2017.

[24] N. Gustafsson, T. Janjić, C. Schraff et al., "Survey of data assimilation methods for convective-scale numerical weather prediction at operational centres," *Quarterly Journal of the Royal Meteorological Society*, vol. 144, no. 713, pp. 1218–1256, 2018.

[25] P. K. S. Sundar and P. C. Deka, *Spatio-temporal classification and prediction of land use and land cover change for the Vembanad Lake System, Kerala–a machine learning approach*, 2021, https://www.researchsquare.com/article/rs-581788/v1.